Low-Cost Markerless Gait Analysis Using a Minimal Human Model

Konstantina Tsintzira[1], Aikaterini Smyrli[*1,2],
Athanasios Mastrogeorgiou[1,2] and Evangelos Papadopoulos[1,2,3]

***Abstract*— This work presents a 2D human model and its use in a novel gait analysis framework, which only requires a stereo camera to produce impressive results for the inverse kinematics, inverse dynamics, as well as ground reaction forces during gait. The model is designed to resemble the human body in the sagittal plane, with anatomical landmarks used as keypoints in the inverse kinematics calculations that yield accurate estimates of the joints' motion during gait. The gait dynamics are formulated in compact form, allowing the simultaneous estimation of internal joint torques, as well as ground reaction forces via the solution of a fully-defined system of linear algebraic equations. The proposed framework offers an affordable alternative to costly gait analysis systems, and can have various applications in robotics and in biomechanics.**

I. Introduction

Gait analysis attracts significant interest due to its wide range of applications in clinical diagnosis, rehabilitation, biomechanics, and most recently, robotics. The study of the human gait cycle and the development of models that can accurately describe human walking have been attractive to many researchers seeking to gain a deeper understanding of human locomotion and to many roboticists with a goal to imitate this naturally observed motion using state-of-the-art humanoid robots [1][2].

An insight into the experimental and analytical methods used in gait analysis is offered in [3], which analyzes joint kinematics and kinetics for the lower limbs during bipedal gait. Mechanical models developed for the simulation of human gait exhibit a range in complexity: from relatively simple models such as the double pendulum [4], to highly detailed ones that model several types of joints found in the human body [5]. The level of modeling detail depends on the requirements of each application: clinical gait analysis may need models of high complexity [3], while for robotic applications, the degrees of freedom of the model are limited to those of the robot under study.

While some researchers have focused on lower limb models [6], a considerable part of the community has opted to develop and use full-body human models [5]. There, the sagittal plane is often on the spotlight, and the dynamic components in the other planes are often simplified [7].

In most studies, to estimate joint forces and torques, gait analysis relies on kinematic data, anthropometric parameters, and force plate data [8][9]. As reported, the requisite kinematic data is acquired using marker-based motion capture systems [8] and [9]. Specifically, special commercial cameras with their proprietary gait analysis software are often used. Most marker-based motion capture systems employ physical markers, the accurate positioning of which along the human body is of paramount importance to a successful gait study. The markers are used to track the position and orientation of body segments accurately.

However, the steep price of commercial systems limits their reach to gait labs, which significantly limits the availability of gait analysis results. The collection of kinematic data using marker-based methods is conducted in controlled environments, which are equipped with the aforementioned motion capture systems, and are staffed by trained personnel. While these methods constitute the state-of-the-art in gait analysis, they entail significant drawbacks beyond the high cost, such as requiring a time-consuming and tiring process for both the personnel and the subject [10][11].

In an attempt to circumvent the shortcomings of marker-based motion capture systems, markerless pose estimation methods have been developed in recent years [12][13]. In these, machine learning methods are used to deduce the human pose by detecting specific keypoints (KPs) on the human body using inexpensive RBG cameras. The human pose can then be used to perform Inverse Kinematics (IK) analysis during human gait [7][14]. For Inverse Dynamics (ID) analysis, the use of force plate data is currently a costly requirement of the state-of-the-art [15][16]. Alternatively, machine learning models [17] and other optimization-based techniques [12][18] have also been used to calculate ID.

In this work, we present a simplified 2D human model that is able to capture the kinematics and dynamics of the human gait. We demonstrate the model using a ZED-2 stereo RGB camera and its accompanying pose tracking framework. The proposed model is used to perform IK and ID analysis of a human subject walking on a treadmill and results are successfully compared to published databases [19]. Special equipment or force plates are not required, which results in a simple and transparent, low-cost alternative to traditional gait analysis systems, constituting a portable solution useful for human motion analysis.

*Corresponding author.

This research work was supported by the project "Applied Research for Autonomous Robotic Systems" (MIS5200632) which is implemented within the framework of the National Recovery and Resilience Plan (NNRP) "Greece 2.0" (Measure: 16618- Basic and Applied Research) and is funded by the European Union-NextGenerationEU.

[1]School of Mechanical Engineering, National Technical University of Athens, Greece. Email: kwnstantinatsintzira@gmail.com

[2]Robotics Institute, Athena Research Center, 15125 Maroussi, Greece. Email: {katerina.smyrli, a.mastrogeorgiou, epapado}@athenarc.gr

[3]HERON - Hellenic Robotics Center of Excellence, Athens, Greece.

II. Human model for Inverse Dynamics

A. Model Description

The developed human model, shown in Fig. 1(a-d), is a 2D model of the human body developed to capture the sagittal plane kinematics and dynamics of human gait. The model includes a torso, a head and two distinct legs and arms, denoted L for the left and R for the right limbs.

This model has 14 Degrees of Freedom (DoF). The first three define the absolute position of the biped's torso, described by the hip coordinates x_{hip}, y_{hip} and absolute orientation θ_{torso}, composing the torso generalized coordinates $\mathbf{q_t} = [x_{hip}, y_{hip}, \theta_{torso}]^T$. Next, each leg's configuration is defined by a set of three relative angles $\mathbf{q_l}_i = [\theta_{1i}, \theta_{2i}, \theta_{3i}]^T$ for the hip, knee and ankle angles of each leg respectively, in which $i = L$ for the left leg and $i = R$ for the right one. Similarly for the arms $\mathbf{q_a}_i = [\theta_{4i}, \theta_{5i}]^T$ are the shoulder and elbow angles. Finally, θ_6 is the relative angle between the head and torso. The above compose the generalised coordinates' vector $\mathbf{q_{14x1}}$:

$$\mathbf{q} = [\mathbf{q_t^T}, \mathbf{q}_{lL}{}^{\mathbf{T}}, \mathbf{q}_{lR}{}^{\mathbf{T}}, \mathbf{q}_{aR}{}^{\mathbf{T}}, \mathbf{q}_{aL}{}^{\mathbf{T}}, \theta_6]^{\mathbf{T}} \quad (1)$$

Fig. 1 also presents the model's KPs, coinciding with the joint positions and distal ends of the model's links. These KPs are an input to the IK analysis. The x and y coordinates of the KPs presented in the figure comprise the 15x1 KP coordinate vectors $\mathbf{x}_{kp}$ and $\mathbf{y}_{kp}$:

$$\mathbf{x}_{kp} = [x_{hip}, \mathbf{x}_{lL}, \mathbf{x}_{lR}, x_{thorax}, \mathbf{x}_{aR}, \mathbf{x}_{aL}, x_{head}]^{\mathbf{T}} \quad (2)$$

where $\mathbf{x}_{li} = [x_{knee-i}, x_{ankle-i}, x_{heel-i}, x_{toe-i}]$ the leg KPs' x-coordinate vector, includes the x-coordinates of the i-leg's knee, ankle, heel, and toe, and $i = \{L, R\}$ for the left and right foot. The coordinate x_{thorax} corresponds to the x position of the thorax. Moreover $\mathbf{x}_{ai} = [x_{elbow-i}, x_{wrist-i}]$ includes the elbow and wrist x coordinates. Finally, the x position of the head link's distal end is x_{head}. Similar definitions apply for $\mathbf{y}_{kp}$. The vectors $\mathbf{x}_{kp}$ and $\mathbf{y}_{kp}$ are a function of $\mathbf{q}$ as well as of the model parameters, also shown in Fig. 1 and analyzed in the next section.

The model's parameters are used to personalize the model to each individual. These are the total body mass and polar moment of inertia of each link m_k and I_k, the length of each of the link l_k, and the position of the Center of Mass (CoM) for each link measuring from the proximal joint r_k. The distinct links of the model are the *torso, femur, tibia, foot, arm, forearm*, and *head*, and are indicated by k. The model is assumed to be symmetrical with respect to the sagittal plane, and there is no distinction between left and right limbs.

Statistically-derived approximations exist for the relationship between some of the model's parameters. Specifically, several approximations exist for the inertial distribution of the human body; in this work, we have applied the estimations found in the widely used OpenSim model Gait2392.

B. Model Dynamics

The dynamics of the model are derived using the Lagrangian method and they are of the general form:

$$\mathbf{M(q)\ddot{q} + C(q, \dot{q}) + G(q) = \Lambda f + T\tau} \quad (3)$$

in which $\mathbf{M_{14x14}}$ is the inertia matrix, $\mathbf{C_{14x1}}$ refers to a vector that includes Coriolis and centrifugal terms, $\mathbf{G_{14x1}}$ includes the gravitational torques and $\boldsymbol{\tau}_{\mathbf{11x1}}$ refers to the vector of unknown internal joint torques applied to the model. There are only 11 such torques, as the absolute DoFs of $\mathbf{q_t}$ are not actuated in the human body. Finally, $\mathbf{f_{10x1}}$ is the vector of the ground reaction wrench, to be analyzed in a later section, and $\mathbf{\Lambda_{14x10}}$ is the ground contact Jacobian matrix. The size of $\mathbf{f}$ will be analyzed in the next section.

To apply the 11x1 $\boldsymbol{\tau}$ to the 14-DoF dynamics model, we left-multiply it by the joint torque Jacobian $\mathbf{T_{14x11}}$:

$$\mathbf{T} = \begin{bmatrix} \mathbf{0_{11x3}} & \mathbf{I_{11x11}} \end{bmatrix}^{\mathbf{T}} \quad (4)$$

where $\mathbf{0}$ is the zero matrix and $\mathbf{I}$ is the identity matrix.

In an ID application, the left-hand side of Eq. (3), $\mathbf{L_{14x1}} = \mathbf{M(q)\ddot{q} + C(q, \dot{q}) + G(q)}$, includes known or measurable elements. However, the right-hand side includes the unknown ground reaction wrench vector $\mathbf{f}$ and joint torque vector $\boldsymbol{\tau}$. Both remain unknown when a gait experiment does not include data from a force plate (which would define $\mathbf{f}$), as is the case for the present study. Here we focus on the estimation of these two vectors.

The ID problem can be written as:

$$\mathbf{L} = \begin{bmatrix} \mathbf{\Lambda} & \mathbf{T} \end{bmatrix} \begin{bmatrix} \mathbf{f} \\ \boldsymbol{\tau} \end{bmatrix} \quad (5)$$

Eq. (5) is an algebraic system of 14 equations and 21 unknowns: 10 in $\mathbf{f}$ -as will be explained in the following section- and 11 in $\boldsymbol{\tau}$.

C. Ground Reaction Forces

When the foot i is in contact with the ground, it is subject to the vertical and horizontal components of the ground reaction force (GRF) acting on the foot, as well as the ground reaction moment. To account for the gradual progression of the foot's center of pressure, as observed in humans while a stance foot is flat on the ground, the model developed assumes *two* distinct forces acting on each foot: $\mathbf{f_i^h} = [f_{xi}^h, f_{yi}^h]$ at the heel position H and $\mathbf{f_i^t} = [f_{xi}^t, f_{yi}^t]$ at the toe T, as shown in Fig. 1(e-f).

This assumption of two contact points per foot is dynamically equivalent to the application of the *sum* of the contact forces on point C, which moves depending on the force distribution between the two contact points H and T. The benefit of this method is that the contact Jacobian $\mathbf{\Lambda}$ refers to points H and T for each foot, and thus remains constant throughout the gait cycle: it is only the relationship between $\mathbf{f_i^h}$ and $\mathbf{f_i^t}$ that has to change, to transfer C forward from the heel to the toe during stance. The ground reaction moment τ_{ci} is a free vector. The ground reaction wrench $\mathbf{f} = [\mathbf{f_L}, \mathbf{f_R}]^{\mathbf{T}}$ is defined:

$$\mathbf{f}_i = [f_{xi}^h, f_{yi}^h, f_{xi}^t, f_{yi}^t, \tau_{ci}],\ i\text{=}L,R \quad (6)$$

It is now evident that $\mathbf{f}$ contains 10 elements.

Depending on the phase of the gait cycle at each time instant, the elements of $\mathbf{f}$ may be subject to further constraints.

During walking, the model alternates between SSP and DSP. In the left leg's *single stance phase* (SSP), the right leg is in swing and no contacts are acting on it, $\mathbf{f}_R = 0$, which can be written:

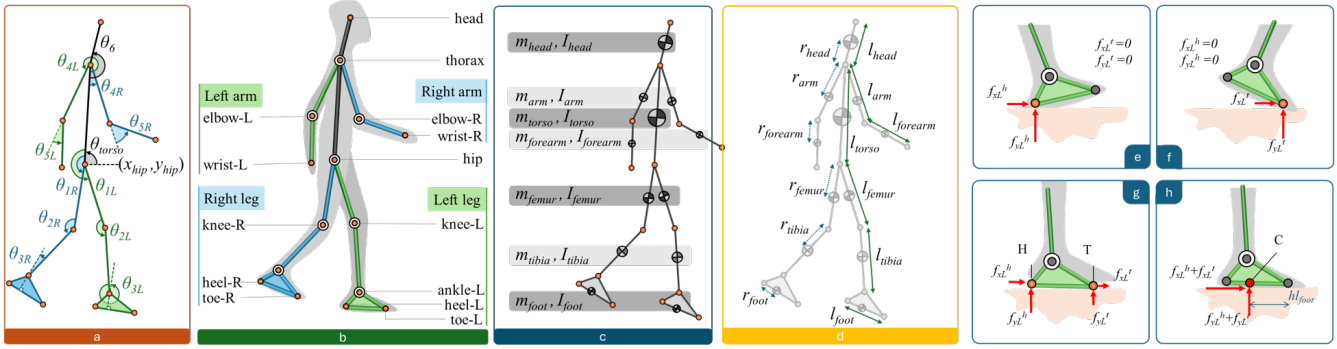

Fig. 1. (a-d) Human model definition. (a) The model's degrees of freedom, (b) joints and KPs, (c) the inertial parameters of the model and (d) link lengths and center of mass positions. (e-h) Ground contact modeling. (e) Heel contact and (f) toe contact. (g) The two components of the GRF acting on the left foot and (h) corresponding total force is applied at point C, which progresses forward according to $h(t)$.

$$\left[\begin{array}{cc} \mathbf{0_{5x5}} & \mathbf{I_{5x5}} \end{array}\right] \mathbf{f} = \mathbf{0} \tag{7}$$

At the same time, the left leg would necessarily be in contact with the ground. We assume the following distribution of forces on the left leg:

$$\mathbf{f_L^h}(1-h) - \mathbf{f_L^t} h = \mathbf{0} \tag{8}$$

in which $h \in [0,1]$ indicates the percentage of the total force that acts at the heel of the foot. When $h = 1$ then $\mathbf{f_i^t} = \mathbf{0}$, corresponding to a heel-only contact following a heelstrike. When $h = 0$ then $\mathbf{f_i^h} = \mathbf{0}$ and the heel is free just before toe off. For values in-between, the sum of contact forces on the left leg is applied at point C. The distance of C from T along the foot is hl_{foot}. Thus, $h(t)$ can be selected to match the desired center of pressure progression during stance.

Eq. (7) and (8) impose 7 algebraic constraints in the solution of (5). They can be written as $\mathbf{W_L f = 0}$ where:

$$\mathbf{W_L} = \left[\begin{array}{ccccc|c} \multicolumn{5}{c|}{\mathbf{0_{5x5}}} & \mathbf{I_{5x5}} \\ \hline 1-h & 0 & -h & 0 & 0 & \multirow{2}{*}{$\mathbf{0_{2x5}}$} \\ 0 & 1-h & 0 & -h & 0 & \end{array}\right] \tag{9}$$

is the GRF distribution matrix for the *left* leg's SSP.

The next phase of normal walking would be a *double stance phase* (DSP) where the weight is transferred from the left toe to the right heel. In this phase, $\mathbf{f_L^h} = \mathbf{0}$, $\mathbf{f_R^t} = \mathbf{0}$, and if $\rho \in [0,1]$ is the ratio of the total GRF that acts on the trailing left leg, then the constraint matrix for the left-to-right DSP is:

$$\mathbf{W_{LR}} = \left[\begin{array}{ccccc|ccccc} 1 & 0 & 0 & 0 & 0 & 0 & 0 & 0 & 0 & 0 \\ 0 & 1 & 0 & 0 & 0 & 0 & 0 & 0 & 0 & 0 \\ 0 & 0 & 0 & 0 & 0 & 0 & 0 & 1 & 0 & 0 \\ 0 & 0 & 0 & 0 & 0 & 0 & 0 & 0 & 1 & 0 \\ \hline 0 & 0 & l & 0 & 0 & r & 0 & 0 & 0 & 0 \\ 0 & 0 & 0 & l & 0 & 0 & r & 0 & 0 & 0 \\ 0 & 0 & 0 & 0 & l & 0 & 0 & 0 & 0 & r \end{array}\right] \tag{10}$$

in which $l = -\rho$ and $r = 1-\rho$. Again, there are 7 constraints appended to the system of Eq. (5).

The corresponding $\mathbf{W_R}$ for the right leg's SSP and the $\mathbf{W_{RL}}$ for the right-to-left DSP are derived similarly.

D. Model Overview

The use of the two-point contact model and the gradual weight transfer between either the heel and toe of one foot or the toe of one foot and heel of the next, has been facilitated via the use of the GRF distribution matrices $\mathbf{W}$.

It was shown that in all phases of walking, there will be a set of 7 algebraic relationships $\mathbf{W}$ between the elements of $\mathbf{f}$. In normal walking, $\mathbf{W}$ will be rotating between $\mathbf{W_L}$, $\mathbf{W_{LR}}$, $\mathbf{W_R}$, $\mathbf{W_{RL}}$. The switch will be performed every time there is either a heel-strike (HS) or a toe-off (TO) event.

With the addition of the GRF distribution constraints $\mathbf{W}$, the system of equations (5) will be:

$$\left[\begin{array}{c} \mathbf{L_{14x1}} \\ \mathbf{0_{7x1}} \end{array}\right] = \left[\begin{array}{cc} \mathbf{\Lambda_{14x10}} & \mathbf{T_{14x11}} \\ \mathbf{W_{7x10}} & \mathbf{0_{7x11}} \end{array}\right] \left[\begin{array}{c} \mathbf{f_{10x1}} \\ \boldsymbol{\tau}_{11x1} \end{array}\right] \tag{11}$$

The new system has 21 equations and 21 unknowns, which can be solved to provide unique solutions for $\mathbf{f}$ and $\boldsymbol{\tau}$. The vector $\mathbf{L}$ depends on $\mathbf{q}, \dot{\mathbf{q}}, \ddot{\mathbf{q}}$, while the matrix $\mathbf{\Lambda}$ depends only on $\mathbf{q}$. Therefore, the estimation of these state variables is required for the ID analysis.

III. Pose Estimation

A. Experimental Setup

In this work, human pose estimation is performed via a vision-based approach. The goal of this approach is to perform an IK and ID analysis of human walking using a low-cost, minimal and portable experimental setup with as short setup time as possible.

An image of our experimental setup is shown in Fig. 2 (a). The minimal setup consists of a treadmill (1.1 m/s, no incline) and a camera system. The user walks on the treadmill at a predefined walking speed, while the camera system captures the resulting motion.

For the experiments, a camera with stereo vision, wide-angle field of view at 120°, and HD video recordings (1280×720) at 60 FPS is needed. To this end, the StereoLabs ZED 2 camera was selected. This camera comes pre-calibrated by the manufacturer: this contributes to a portable and easily configurable experimental setup. Most importantly, this camera is compatible with its SDK framework, which offers neural network-based 3D Body KP Tracking. Fig. 2 (b) presents the dual camera view.

B. Body Keypoints and Model Fitting

The Body Tracking functions of the camera's SDK have been utilized, following minor modifications in the open-source code provided by the manufacturer. The Body Tracking features of the SDK produce a video recording of the

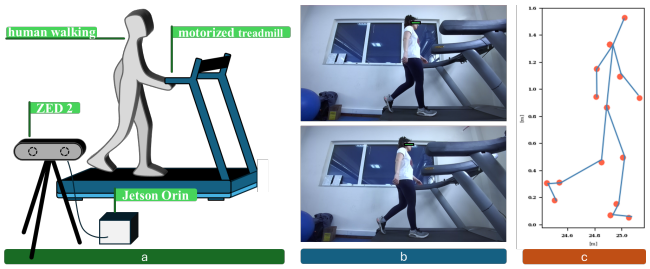

Fig. 2. (a) Experimental setup. (b) Stereo camera frames during the experimental process using the ZED-2 camera. (c) Sagittal plane projection of body KPs using ZED SDK (red dots), and body fitting (blue lines).

walking trial, along with a JSON file that tracks the 3D trajectories of 34 body KPs. Out of these, a subset of 15 KPs is extracted, corresponding to our model's KPs. The projection of these select KPs in the sagittal plane, $\mathbf{x}_{kp}^{z}$ and $\mathbf{y}_{kp}^{z}$ is used as an input to the IK analysis. Fig. 2 (c) shows the selected 15 KPs.

The data obtained from $\mathbf{x}_{kp}^{z}$ and $\mathbf{y}_{kp}^{z}$ is used to determine the model's link lengths l_k, by averaging the Euclidean distance between specific body KPs throughout an experiment. In this way, this set of model parameters is precisely tailored to the individual user. The rest of the model's parameters are set based on the statistical approximations specified in Section II.B. Following this automated parameter fitting procedure, the personalization of the model is complete and the model is ready to be deployed for the gait analysis study.

Finally, the camera KPs $\mathbf{x}_{kp}^{z}$ and $\mathbf{y}_{kp}^{z}$ are used to determine the model's configuration at each timestep. Given that the model's link lengths have been set as the average value of all recorded link lengths, it is expected that the camera KPs $(\mathbf{x}_{kp}^{z}(t_i), \mathbf{y}_{kp}^{z}(t_i))$ and model KPs $(\mathbf{x}_{kp}(t_i), \mathbf{y}_{kp}(t_i))$ will not coincide at each timestep t_i, but they will remain close. Additionally, the 15 sets of model KPs provide redundant information, when the goal is to determine the 14 DoF of (1). Consequently, a non-linear least squares optimization is performed to fit the model to the KPs at each time instant t_i, by minimizing the cost function $\mathscr{F}_c$, which is the Euclidian norm of the KP fitting errors:

$$\mathscr{F}_c = \|\Delta_x - \Delta_y\|_2 \tag{12}$$

$$\Delta_x = \mathbf{x}_{kp}^{z}(t_i) - \mathbf{x}_{kp}(t_i) \tag{13}$$

$$\Delta_y = \mathbf{y}_{kp}^{z}(t_i) - \mathbf{y}_{kp}(t_i) \tag{14}$$

are 15x1 coordinate errors in the x and y directions.

The optimization is performed in a loop for all recorded times t, providing a timeseries $\mathbf{q}(t)$ that replicates the recorded KP trajectories. Fig. 2 (c) presents a comparison between camera KPs and the optimized model configuration for one time step.

IV. Results and Discussion

A. Results

The IK process involves the estimation of the model's generalized coordinates $\mathbf{q}(t)$ using measurable trajectories. This has been performed in Section III.D using the least squares optimization method.

The obtained joint trajectories $\mathbf{q}(t)$ are significant in gait analysis studies. Even though the specific joint trajectories may be unique to an individual's gait, specific gait impairments may be diagnosed from recorded joint trajectories that majorly deviate from the average human joint trajectories.

Fig. 3(a) presents the hip, knee, and foot joint trajectories $\mathbf{q}_{lL} = [\theta_{1L}, \theta_{2L}, \theta_{3L}]^{\mathrm{T}}$ for the left foot of a healthy female human volunteer (30 y.o., 164 cm, 58 kg, no previously known musculoskeletal disorders, informed consent provided), as these were recorded using the methods presented in this paper. The figures also include the average joint trajectories obtained from [19] and the corresponding RMSE, demonstrating the effectiveness of the proposed approach in capturing the IK of the lower-limb joints.

Following the IK analysis, the joint angles are twice differentiated numerically to produce the joint velocities $\dot{\mathbf{q}}(t)$ and accelerations $\ddot{\mathbf{q}}(t)$. These are input into Eq. (11) which is solved once for every timestep, producing estimates of the joint moments $\boldsymbol{\tau}$ and ground reactions $\mathbf{f}$. A sigmoid function [20] was used as the ground progression function h. Fig. 3(b) presents the lower limb normalized joint torques per kg predicted by the developed framework. Average values of these joint torques as obtained from the database in [19] are also included in Fig. 3(b) to act as a reference. The Root Mean Square Error (RMSE) of the two plots are also presented in the figure.

Finally, the horizontal and vertical GRF acting on the left foot during one gait cycle are presented in Fig. 3(c). These are calculated as the sum of heel and toe force components $\mathbf{f}_{\mathbf{L}}^{\mathbf{h}} + \mathbf{f}_{\mathbf{L}}^{\mathbf{t}}$ in the x and y direction respectively, obtained from solving (11) for $\mathbf{f}$. Average database values for the GRF are also plotted on the same plots, as obtained from [19], along with the calculated RMSE.

B. Discussion and Future Work

As shown in the plots of Fig. 3(a), the developed methodology for IK and ID analysis of human gait has produced valid estimations of the joint trajectories, joint internal torques, and GRF.

The obtained results present close proximity to the respective average values for treadmill walking at the same velocity $u = 1.1[m/s]$, as these were obtained from [19].

Minor divergence from the averaged database curves in the kinematic and dynamic behavior may be observed in some of the results; this is expected to some extent due to the uniqueness of an individual's gait patterns when compared to averaged values. Another source of divergence may be the simplicity of the proposed 2D model, which is an approximation of the complex dynamics of the human body, and the limitations of the low-cost motion capture setup used.

For IK, the detected joint motion demonstrates significant resemblance to the averaged database values. Small differences may be attributed to the individual's gait, the pose detection framework selection and the KPs' translation to the model's joint positions for the IK analysis. In the future, a custom image-based pose detection network may need to be designed and trained specifically for gait analysis, to lead to an improved estimation of anatomical joint locations.

For ID, the model selection plays a significant role in the accuracy of the results. Based on the findings of this study,

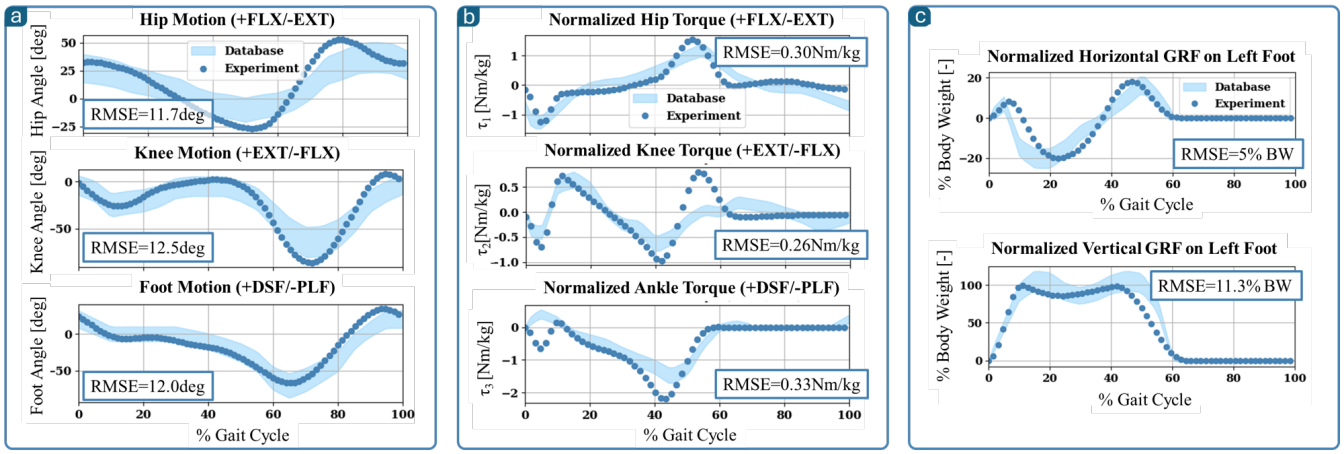

Fig. 3. Joint trajectories (a), normalized per kg joint torques (b), and GRF (c) of the left leg from IK and ID analysis, compared to database averages from [19].

a solid foot may be an over-simplification, not fully able to capture the stance dynamics, even when accounting for gradual weight progression as was performed here. In the future, we plan to introduce some compliance to emulate the motion between hindfoot and metatarsals.

Finally, the GRF estimated in this study are indicative of the literature values. The reliable calculation of GRF through Lagrangian dynamics constitutes an effective and efficient approach that eliminates equipment requirements such as force plates or IMUs.

The initial results presented here are encouraging, with successful comparisons to published database averages. Notably, the method still lacks the medical-grade precision of the current SOTA set by marker-based systems. However, the highlights of this work are the minimal equipment requirements, low cost, simplicity and transparency of the developed approach, that pave the way towards universally available gait analysis tools for use in robotics applications as well as medical pre-screening.

Currently underway is the development of a custom, gait-optimized pose-detection framework to refine inputs and improve results [21]. Immediate next steps include multi-participant experiments and direct comparison with a medical-grade motion-capture system to quantify errors and fine-tune the model for highly reliable results.

V. Conclusion

This work applied a simple human model to gait analysis: the model was fully specified, and IK and ID solutions were formulated, providing analytical, closed-form solutions for joint angles, internal torques, and GRF. A stereo camera with pose-tracking software served as the motion-capture system. The results demonstrate accuracy, matching a public dataset of treadmill gait kinematics and kinetics in healthy adults.

References

[1] H.I. Lin and C.C. Chou, "Humanoid robot motion imitation using Kinect," *Int. Conf. on Advanced Robotics and Intelligent Systems*, Taipei, Taiwan, pp. 1-4, 2015.

[2] W. Suleiman, et al., "On human motion imitation by humanoid robot," *IEEE International. Conf. on Robotics and Automation*, Pasadena, CA, USA, pp. 2697-2704, 2008.

[3] A. Cappozzo, "Gait analysis methodology," *Human Movement Science*, vol. 3, no.(1-2), pp. 27 - 50, 1984.

[4] H. Wahrenberg, et al., "Dynamic loading in the human knee joint during voluntary active impact to the lower leg," *Scandinavian Journal of Rehabilitation Medicine*, vol. 10, no.2, pp. 93-98, 1978.

[5] L. Ren, et al., "Whole body inverse dynamics over a complete gait cycle based only on measured kinematics," *J. of Biomechanics*, vol. 41, no.12, pp. 2750 - 2759, 2008.

[6] J. Apkarian, "A Three- dimensional kinematic and dynamic model of the lower limb," *J. of Biomechanics*, vol. 22, no.2, pp. 143 - 155, 1989.

[7] J. Stenum, et al., "Two-dimensional video-based analysis of human gait using pose estimation," *PLOS Computational Biology*, 2021.

[8] A. Leardini, et al., "A new anatomically based protocol for gait analysis in children," *Gait & Posture*, vol. 26, pp. 560 – 571, 2007.

[9] A.G. Schache, et al., "On the expression of joint moments during gait," *Gait & Posture*, vol. 25, no.3, pp. 440 - 452, 2007.

[10] M. Moro, et al., "Markerless vs. Marker-Based Gait Analysis: A Proof of Concept Study," *Sensors*, vol. 22, 2022.

[11] J. Yang and K. Park, "Improving Gait Analysis Techniques with Markerless Pose Estimation Based on Smartphone Location," *Bioengineering*, vol. 11, no.2, 2024.

[12] Uhlrich, S. D. et al., "OpenCap: Human movement dynamics from smartphone videos", *PLoS comp. biology*, vol. 19, no. 10, 2023.

[13] Z. Cao, et al., "Realtime Multi-person 2D Pose Estimation Using Part Affinity Fields," *IEEE Conf. on Computer Vision and Pattern Recognition*, Honolulu, HI, USA, pp. 1302-1310, 2017.

[14] E.P. Washabaugh, et al., "Comparing the accuracy of open-source pose estimation methods for measuring gait kinematics," *Gait & Posture*, vol. 97, pp. 188-195, 2022.

[15] S.L. Delp, et al., "Open-source Software to Create and Analyze Dynamic Simulations of Movement," *IEEE Trans. on Biomedical Engineering*, vol. 54, pp. 1940-1950, 2007.

[16] T. Huang, et al., "Comparison of kinematics and joint moments calculations for lower limbs during gait using markerless and marker-based motion capture," *Frontiers in Bioengineering and Biotechnology*, vol. 12, 2024.

[17] M. Mundt, et al., "Prediction of ground reaction force and joint moments based on optical motion capture data during gait," *Medical Engineering & Physics*, vol. 86, pp. 29-34, 2020.

[18] Xie, K., et al., "Physics-based human motion estimation and synthesis from videos", *IEEE/CVF Int. Conf. on Computer Vision*, pp. 11532-11541, 2021.

[19] C.A. Fukuchi, et al., "A public dataset of overground and treadmill walking kinematics and kinetics in healthy individuals," *PeerJ*, 2018.

[20] Samadi B, et al., "Decomposition of three-dimensional ground-reaction forces under both feet during gait", *J. Musculoskelet Neuronal Interact.* 2017.

[21] Stavrakakis O., et al., "Guidelines For Optimal Human Mesh Generation Using Deep Learning-Driven Avatar Reconstruction For Gait Analysis," *IEEE-RAS Int. Conf. on Humanoid Robots*, 2024.

Acknowledgment

This work was partially funded by the European Union under Horizon Europe (grant No. 101136568 - HERON).

Funded by the European Union